Available online at www.sciencedirect.com
ScienceDirect
Journal of Photochemistry and Photobiology A: Chemistry 187 (2007) 97–104
Journal of Photochemistry and Photobiology A:Chemistry
www.elsevier.com/locate/jphotochem

Hydrogen photoproduction over new catalyst $CuLaO_2$

S. Saadi, A. Bouguelia, A. Derbal, M. Trari *

Laboratoire de Stockage et de Valorisation des Energies Renouvelables, Faculté de Chimie, (U.S.T.H.B), BP 32 16111 Algiers, Algeria

Received 3 June 2006; received in revised form 13 September 2006; accepted 30 September 2006
Available online 12 October 2006

Abstract

Excellent quality $CuLaO_2$ has been synthesized through solid reaction in evacuated silica tubes and the delafossite structure was refined in the space group $R\bar{3}m$. The oxide is thermally stable up to ∼200 °C, above ∼610 °C it converts irreversibly to $CuLa_2O_4$. The conduction band (−1.99 V_{sce}) lies below H_2O/H_2 level leading to a thermodynamically favorable H_2-photoevolution with concomitant oxidation of X^{2-} (=S^{2-} or SO_3^{2-}). The surface platinization improved the activity by increasing the rate constants of X^{2-} oxidation. The redox kinetic is relatively fast with SO_3^{2-} whereas the electrochemical system S^{2-}/Pt behaves irreversibly and where the polarization is mainly of activation. The charge carriers move in a narrow conduction band made up primarily of Cu 3d orbitals. The rate determining step is the supply of electrons at the interface because of their low electron mobility. The system is optimized with respect to some physical parameters and the best photoactivity (47 ml g^{-1} h^{-1}) was obtained with SO_3^{2-} at pH ∼8. In a closed reactor, the oxidized species namely $S_2O_6^{2-}$ and S_n^{2-} tend to stop the H_2 formation because of their competitive reductions with H_2O. Moreover, the formation of S_n^{2-} leads to a less transparent electrolyte that permits fewer photons to reach the crystallites.

Keywords: Delafossite; H_2-photoevolution; Platinization; Polysulfide; Electron mobility

1. Introduction

Various alternatives to achieve water splitting upon visible light have been studied [1–3]. Hydrogen photogeneration over semi-conductor (SC) powders has been one of the central topics in the energy research [4]. It has attracted much attention as a way of storing solar energy and it is still the subject of intense researches in the sense that simple photoelectrochemical (PEC) systems [5] offer numerous advantages with respect to higher priced electrochemical devices. For a p-type SC to be used as photocathode, it must combine (i) a sufficient light absorption in the visible region, (ii) a long-term chemical stability, (iii) a large band bending, and (B) under working conditions; the last point implies a flat band potential (V_{fb}) as positive as possible. When a p-type SC is brought in contact with a redox electrolyte, equilibrium is established with equalization of electrochemical potentials of both phases. A transfer of minority carriers occurs from the bulk of SC to the interface and an upward bending of electronic bands near the surface results. The separation of photogenerated electron–hole (e^-/h^+) pairs occurs through the internal electric field that is formed spontaneously within the space charge region (SCR) of length (W) [6]. Sunlight may be converted and stored directly into chemical energy and our program consists of investigating materials for bias-free photoelectrodes focused mainly on H_2 production [7]. Generally, the stable oxides possess large forbidden gap (E_g), exceeding sometimes 3 eV, a negative parameter with regard to practical use whose photosensitivity is restricted to UV region accounting only for ∼4% of sun spectrum at sea level (one sun AM1.5). To that end, studies have been directed toward search of oxides with new crystalline and bands structure. The layered $Cu^+M^{3+}O_2$ crystallizing in the delafossite structure offer this eventuality and begin to receive scientific attention owing to their interesting properties [8,9], M being a rare earth or a 3d metal. These oxides are low mobility polarons, hopping SC where both valence (VB) and conduction (CB) bands are of Cu 3d character. They occur mostly as p-type inhibiting thus chemical attack in aqueous electrolytes. H_2 evolution depends on the energetic position of CB with respect to H_2O/H_2 couple and a further attractive characteristic with such oxides is that the potential V_{fb} is pH-insensitive, attributed to the non-adsorption of ions (*e.g.* OH^-, H^+). We have taken advantage of this property and

* Corresponding author. Tel.: +213 21 24 79; fax: +213 826324602.
E-mail address: mtrari@caramail.com (M. Trari).

1010-6030/$ – see front matter © 2006 Elsevier B.V. All rights reserved.
doi:10.1016/j.jphotochem.2006.09.017

by varying the pH of the solution, the H_2O/H_2 level can then be raised above CB allowing an efficient carrier transfer by reducing the H_2-overpotential η[1]. This strategy has been successfully attempted in our laboratory with the water photoreduction over $CuCrO_2$ [5] and more recently on $CuYO_2$ [10].

The potential of O_2/H_2O couple over $CuMO_2$ ($\sim$1.5 V_{SCE}) is too positive ascribed to large O_2-overpotentials and oxygen does not evolve through VB process. For that reason, water reduction is coupled with a parallel oxidation of inorganic pollutant. The conversion of sulfides and sulfites into less harmful compounds to set up the local electrochemical cell is a desirable goal. The stored energy is then the free enthalpy difference between the end products. On the other hand, the photoactivity can be improved significantly by partial coverage with precious metal because of their large rate constants for water oxidation. Pt remains the material of choice in such applications and the reactions proceed with small overvoltages [11]. In addition, the H_2 liberation lowers the potential barrier height of SC/noble metal junction where electrons can easily pass through the interface [12]. Among delafossites that have been considered, attention may be directed towards $CuLaO_2$. This oxide is part of the program on the photoelectrochemistry of $CuMO_2$ family. To our knowledge, there are no papers in the literature concerning either the electrochemistry or the practical application with this cuprous oxide much except for our recent paper [manuscript in preparation]. In order to back this statement up and in continuation with this interesting class of materials, we report on the first results of $CuLaO_2$ as candidate for H_2-photoelectrode. $CuLaO_2$ was synthesized and characterized electrically and photoelectrochemically. Its CB is predicted to be more negative than the H_2O/H_2 potential leading to a thermodynamically favorable H_2-photoevolution.

2. Experimental

High quality $CuLaO_2$ powder was elaborated by solid-state reaction from extra pure La_2O_3 and Cu_2O (purity >99%). Stoichiometric amounts were mixed in an agate mortar, pelletized and sealed in silica tubes under dynamic vacuum ($\sim$1 mbar) to preclude formation of $CuLa_2O_4$. The pellets were heat treated at 960 °C and then quenched by dropping in water. The process of grinding and firing was repeated to ensure a complete reaction; the compactness was $\sim$75% with good mechanical properties. La_2O_3 and Cu_2O were fired respectively, at 800 °C in air and 500 °C under vacuum just prior use and handled in a glove box filled with argon because of their strong moisture sensitivity. Cu_2O possess large quantum efficiency and was removed by soaking the powder in 5N NH_4OH. This procedure was repeated a number of times until no further Cu^{2+} was detected. For PEC characterization, we did not succeed in preparing $CuLa_{0.98}Ca_{0.02}O_2$ by a similar method. Data of X-ray diffraction were obtained at 0.05° interval over an angular range 2θ of 25–85° using a monochromatized Cu Kα radiation ($\lambda = 0.154178$ nm). Silicon was used to calibrate the 2θ angles and the lattice constants were refined by the least square method. The density d_{exp} was determined by the displacement method in bromoform because of its wetting property.

Iodometric titration has been used to evaluate the mean valency of copper. Oxide ($\sim$30 mg) was dissolved in 3N HCl containing an excess of KI. The liberated iodine was then titrated by a standard Na_2SO_3 solution. The oxygen content was determined by thermal analysis (TGA) in air up to 900 °C with a heating rate of 3 °C min^{-1} using a thermoanalyser (Setaram Setsys 16/18). The differential scanning calorimetry (DSC) was performed in the heating direction at a rate of 3 K min^{-1} in the range (50–390 °C). The reflectance diffuse spectra was recorded on a Jasco V-530 UV–visible spectrophotometer attached with a reflectance accessory; E_g was calculated using the wavelength of absorption edge. For corrosion tests, dissolved copper was analyzed by atomic absorption on a Pye Unicam spectrometer 230.

Electrochemical measurements have been carried out using a "three-electrode device", $CuLaO_2$ photocathode, a Pt counter electrode and a saturated calomel electrode to which all potentials are quoted. The light source was a 500 W halogen lamp.

The photocatalytic reactions were performed in a double-walled cell whose temperature was maintained at 48 °C (within ±0.1 °C) using a temperature controller (Julabo III). 50 mg of catalyst was suspended by magnetic stirring in 40 ml of X^{2-} solution and illuminated by a 650 W halogen lamp. The imprecision was caused mainly by the cell sitting in slightly different positions. The cell was positioned in a standard fashion to keep a constant photon flux. The pH of solutions was regulated by KOH and HNO_3 using a pH meter (Schott CG825, accuracy ±0.01 units). Before each run, the newly prepared solution was purged with nitrogen for at least 30 min and sealed off with a glass cap. Hydrogen in the outgoing gas was positively identified by gas chromatography and no other gas was detected. The amount of H_2 was measured volumetrically by displacement of water due to the pressure developed inside the cell; a blank test without catalyst was carried out in the same conditions. The absorbance of yellow polysulfides S_n^{2-} was measured colorimetrically at $\lambda_{max} = 520$ nm. The solutions were made up from analytical reagents and demineralized water. The surface platinization of $CuLaO_2$ was carried out from unfiltered UV irradiation in acetic acid containing $H_2PtCl_6 \cdot xH_2O$, purchased from Merck Company, according to Ref. [21].

3. Results and discussion

3.1. Structural and transport properties

$CuLaO_2$ gave a single phase X-ray pattern with an excellent crystallinity (Fig. 1), indexed to a hexagonal symmetry. The lattice constants $a_h = 0.38350(0)$ nm and $c_h = 1.7105(9)$ nm are in perfect agreement with those of previous authors [14] or in the rhombohedral description $a_r = 0.6117(0)$ nm and $\alpha = 36.54°$. The experimental density (5.20) agrees with that calculated on the basis of three formula weights per unit cell (5.36). The comparison of observed and calculated d-spacing and corresponding $h\,k\,l$ indices are listed in Table 1. The structural refinement was

[1] η is not the classical overpotential but the difference between the bands edges and redox couples, it is function of E_g and E° of redox couple but current independent.

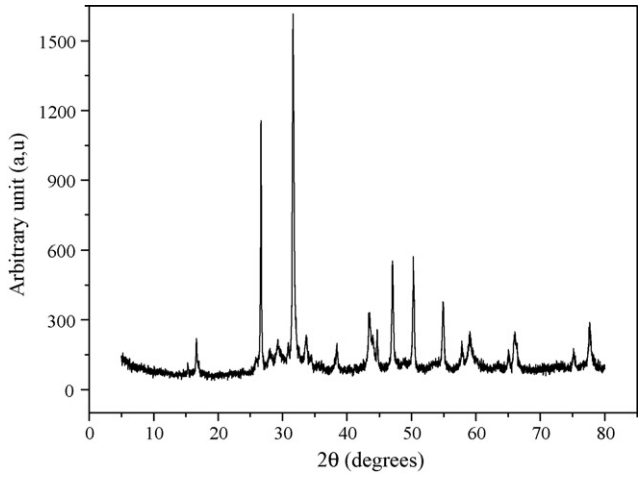

Fig. 1. XRD pattern of $CuLaO_2$ synthesized by solid-state reaction. All peaks are indexed on the basis of a hexagonal unit cell.

made by isotypying with the space group $R\bar{3}m$ and the position parameters of $CuAlO_2$ [15]. Selected interatomic lengths and bond angles are given in Table 2. The $CuLaO_2$ structure is highly anisotropic and contains infinite sheets of edge shared LaO_6 octahedra interleaved with layers containing exclusively Cu^+. Each copper is hexagonally coordinated by six other coppers in the basal plan and linearly coordinated to two oxygen forming

Table 1
comparison of observed and calculated *d*-spacing and corresponding *h k l* indices

Observed *d* (Å)	Intensity (%)	*d* (calculated) (Å)	*h k l* (calculated)
5.71	13	5.70191	003
3.20	4.8	3.26	011
2.85	10	2.85098	006
2.62	17.3	2.62307	014
2.38	7.4	2.38301	105
1.97	2	1.96831	017
1.91	20	1.91750	110
1.81	6	1.81748	113
1.6533	2	1.65283	021
1.6306	5.01	1.63016	022
1.5914	8.88	1.5911	116
1.5486	6.13	1.54799	024
1.5213	4.3	1.52073	0110
1.4943	2.06	1.49392	025
1.4258	2	1.42549	0012
1.4087	1.18	1.40834	0111
1.3736	1.68	1.37349	027
1.3494	1.17	1.34988	119
1.3118	2.58	1.31154	028
1.252	1.81	1.25193	121
1.2420	6.89	1.24199	122
1.2046	3.53	1.20448	124
1.1917	2.46	1.1915	2010
1.1786	2.38	1.17847	215
1.1443	2.95	1.14400	1112
1.1168	1.48	1.11659	217
1.1061	3.13	1.10707	030
1.0867	1.99	1.08677	033
1.0826	3.13	1.08253	128
1.0153	1.5	0116	1.0769
1.012	2.38	1.01203	2110
1.0097	1.77	1.00841	037

Table 2
Listing of bond distances (nm) and angles (degrees)

Bond	Bond distances (nm)	Angles (degrees)
Cu–O	0.1825	–
La–O	0.2440	–
O–Cu–O	–	180.0
O–La–O	–	103.6
O–La–O	–	76.4
O–La–O	–	180.0

$(CuO_2)^{3-}$ "dumb-bell" parallel to *c*-axis, responsible of the photoluminescence which involves $3d^9 4s \rightarrow 3d^{10}$ transitions not allowed for free ion [16]. The yellow color of $CuLaO_2$ is ascribed to a charge transfer through interbands excitation with d–d transition characteristics. Such a crystalline structure is compatible with the good chemical stability. The percentage porosity, calculated from $P = 100(1 - d/d_x)$, works out to be 76%, d and d_x being respectively, the apparent and X-ray densities. The mean crystallite size L, determined from the width β at half maximum of intense X-ray line (0 1 2) through the relation $L = 0.94\ \lambda(\beta \cos\theta)^{-1}$, averaged 62 nm, θ being the angle diffraction. Accordingly, the specific surface area S_{sp} ($\sim$18 m^2/g) was deduced from d assuming nonporous and spherical crystallite shape through the relation ($S_{sp} = 6/Ld_{exp}$).

$CuLaO_2$ is expected to be diamagnetic; however, the thermal variation of the magnetic susceptibility $\chi(T)$ (Fig. 2) exhibits a slight paramagnetism attributed to Cu^{2+} originated from oxygen insertion in the layered lattice. The amount of Cu^{2+} was estimated from the Curie constant C (manuscript in preparation). The C-value (=0.003) is $\sim 10^{-2}$ of 0.375 for Cu^{2+} free spins ($S = 1/2$ and $g = 2$) and corresponds to 0.265 mol% O^{2-} in good agreement with the formulation $CuLaO_{2.02}$. The presence of Cu^{2+} is supported by a wide ESR line ΔH_{pp} of $\sim$1000 G.

In contrast to other delafossites, $CuLaO_2$ was not characterized photoelectrochemically and information concerning its electrochemistry is lacking. Pure $CuLaO_2$ cannot be used as electrode due its electrical resistivity $\rho_{300K} > 10^6\ \Omega$ cm. Attempts have been made to incorporate calcium on the La-sublattice. The unsuccessful synthesis of $CuLa_{0.98}Ca_{0.02}O_2$ can-

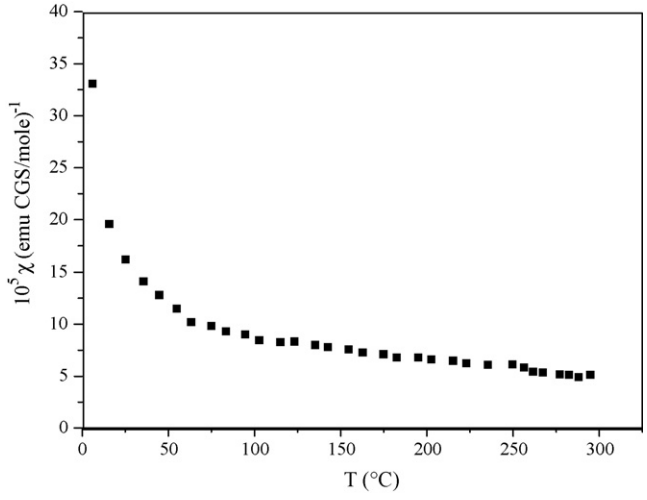

Fig. 2. The thermal variation of the magnetic susceptibility (χ) of $CuLaO_2$.

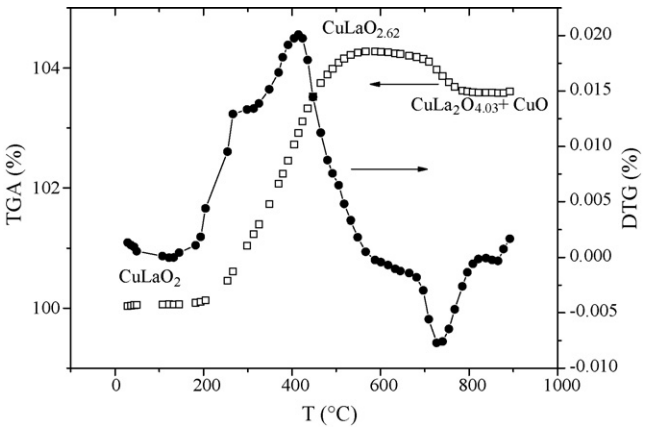

Fig. 3. Combined TGA–DTG plots of $CuLaO_2$ performed in air.

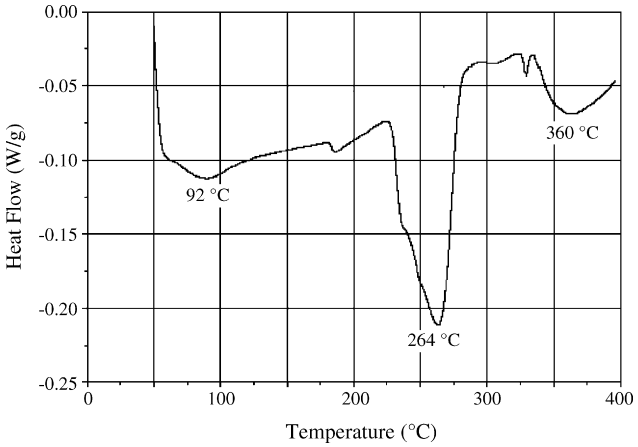

Fig. 4. Differential scanning calorimetry (DSC) of $CuLaO_2$.

not be understood from size consideration in spite of close proximity of ionic radii of La^{3+} (0.103 nm) and Ca^{2+} (0.100 nm) in octahedral sites [17]. However, it has been shown that $CuLaO_2$ irreversibly intercalate O^{2-} species at moderate temperatures [14]. Considering the charge neutrality, the slight over-stoichiometry would induce p-type conductivity; the value of $\rho_{300K} = 1240\ \Omega$ cm allows the oxide to be used as electrode. The low hole mobility ($\sim 10^{-5}$ m^2 V^{-1} s^{-1}) is in conformity with a mechanism of small polaron hopping between mixed valences copper. The ions $Cu^{+/2+}$ are in direct interaction and do not overcome a further potential barrier due to oxygen polyhedra (see delafossite structure).

3.2. Thermal and chemical stabilities

The TGA and differential thermal gravimetric (DTG) performed in air are shown in Fig. 3. The first stage of oxidation starts at ~200 °C to reach a maximum at 565 °C accounting for 4.21% and corresponding to $CuLaO_{2.62}$. Copper exhibits three oxidation states and oxygen is accommodated in the layered lattice leading to a mixed valency $Cu^{2+/3+}$ as required by the electroneutrality condition. Up to 620 °C, the oxide has noticeable broader peaks and therefore is less crystalline than the 550 °C sample. Above 660 °C, it undergoes an irreversible reduction into $CuLa_2O_{4.03}$ and CuO as final products. A total weight loss of 3.54% was noted up to 800 °C in agreement with that calculated (3.41%). The well-known stoichiometry of La_2O_3 allows an accurate determination of oxygen content (2.018) (Fig. 3). The TGA plot is correlated by DSC measurements where clear anomalies exist in the DSC curve (Fig. 4). The plot shows endothermic peaks; the first one at 92 °C is attributed to departure of adsorbed water. The peak located at 264 °C corresponds to the beginning of oxygen insertion whereas that centred at 360 °C can be attributed to oxygen intercalation in the crystallographic sites.

It is helpful to outline that the influence of silica tube volume (~20 cm^3) on the oxygen over-stoichiometry for $CuLaO_{2+\varepsilon}$ (~400 mg) is negligible; it introduce only ~0.16 μmol of O_2 which corresponds to $\varepsilon = 2 \times 10^{-4}$. This value disagrees with that obtained from iodometry and magnetism (see below); the nominal oxidation state for Cu of 1.02 corresponds to ε-value of 0.01.

The interfacial exchange reactions are slow; consequently large surface area and much longer duration are required for measuring the corrosion rate by chemical analysis. The dissolution rate of $CuLaO_2$ powder in 1 M KCl measured by atomic absorption of dissolved Cu^{2+}, after an 8-month period, was equal to 6×10^{-4} mol m^{-2} day^{-1}. However, in the absence of appropriate electro active species, the corrosion taking place under irradiation was verified electrochemically. Cu^{2+} released into the solution has been detected analytically in presence of ammonia by formation of the blue complex $Cu(NH_3)_6^{2+}$. The photocorrosion rate was connected with H_2-production; it corresponds to the rate of holes accumulation (see below) and was found to be 26.4×10^{-4} mol^{-1} m^{-2} day^{-1}.

3.3. Optical and photoelectrochemical properties

The highest full band (VB), derived from CuO_2^{3-} units is ~2 eV positive of O^{2-}-2p levels whereas the lowest empty level is the antibonding σ^* CB, some 5 eV above the O^{2-}-2p level. Lanthanum is less acidic and its electropositive character leads to a stronger covalency of Cu–O bond and consequently to a larger

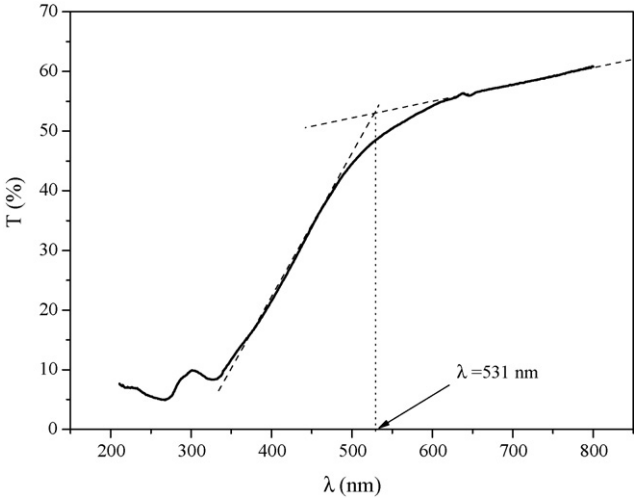

Fig. 5. Diffuse reflectance spectra of $CuLaO_2$.

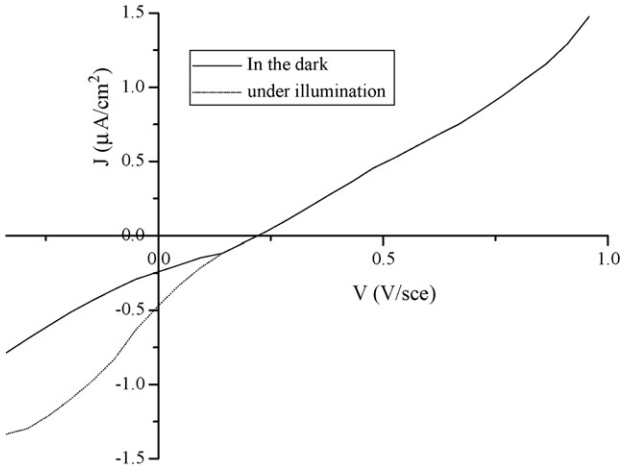

Fig. 6. The $J(V)$ curve of $CuLaO_2$ in the dark and under illumination upon visible light. Electrolyte 1 M KOH, scan rate 5 mV s^{-1}.

destabilization of CB of Cu: $3d_{z2}$/4s parentage. VB is made up of non-bonding t_{2g} orbital and remains nearly constant regardless of the nature of M^{3+} ion. This results in a smaller electron affinity (EA) and a larger gap E_g; indeed $CuLaO_2$ possess the larger E_g among $CuMO_2$. The absorption edge of the reflectance diffuse spectra is well defined, which is expected for direct transitions (Fig. 5). It was obtained by the intersection of the line tangent of the initial rise in the transmittance curve and the saturation level. The absorption onset allowed us to determine the E_g-value at 2.33 eV (Fig. 5).

The PEC characterization was done in N_2 purged 1 M KOH. The electrode was illuminated with white light; the photocurrent starts to flow at ~0.14 V (Fig. 6) and its cathodic direction confirms the p-type semi-conductivity. The potential of photocurrent onset V_{on}, assimilated to V_{fb} is slightly lower than that of isostructural $CuYO_2$ [18] and the difference comes from the larger EA of yttrium (Fig. 6). The position D of VB can be correlated to the potential V_{fb}[2] corrected to pzzp [19]:

$$D = 4.75 + eV_{fb} + \Delta E + \Delta_{pH} \quad (1)$$

ΔE being the activation energy and the adopted value (0.2 eV) appears to be optimal in most delafossites [20], Δ_{pH} is a small correction due to the double layer independent of pH which can be neglected. D equal to 5.1 ± 0.1 eV is in the range 5.0–5.2 eV, typical for $CuMO_2$ in which VB arises from Cu 3d wave functions in contrast to O^{2-}: 2p type VB positioned at ~7.2 eV below vacuum. The value of CB ($-1.99\ V_{SCE}$) lies below H_2O/H_2 level and should give rise to a thermodynamically favorable H_2-photoevolution.

3.4. Photoactivity

The H_2-formation occurs at potentials cathodic of ~−1 V over $CuMO_2$ [15] and the ability of p-type specimen to operate with no external bias depends on the potential of CB with respect to H_2O/H_2 couple. The electron exchange is determined by the relative positions of unoccupied states pertained to adsorbed H_2O and CB. An efficient charge transfer is expected if both energetic states show a good overlap. A remarkable feature of $CuLaO_2$ resides in its electronic bands that are pH-independent. The PEC process of H_2-formation is thermally activated and all experiments were conducted at (48 ± 0.1) °C. Increasing the temperature improves the photoactivity because of more efficient mass transfer in the electrolyte and carriers transport within the diffusion length L_D by enhancing their mobility. The amount of evolved H_2 at 50 °C was about two fold greater than that obtained at room temperature. Higher temperatures resulted in electrolytes losses by vaporization.

As mentioned in introduction, the charge separation depends on the existence of SCR which introduces a junction electric field in the depletion layer. The band bending B at the interface must be large enough to allow a good separation of e^-/h^+ pairs. To have a zero e^-/h^+ recombination, a maximal B-value ($= |V_{fb} - E^0_{red}|$)) is desirable in a darkness situation. Changing the reducing agent is an indirect way to polarize the crystallite and to extend the length W by increasing the quantity B. In such a case most electrons reaching SCR are transferred to adsorbed water followed by H_2-liberation;

$$W = \left\{ 2\varepsilon\varepsilon_0 \frac{B}{eN_D} \right\}^{0.5} \quad (2)$$

ε and ε_0 are respectively, the dielectric constants of material and free space, e the electron charge and N_D the doping density. ε is unknown in our case but the low doping N_D produce a large width W which is of same order of magnitude than the crystallite size d, so the efficiency is expected to be high. On the other hand, p-$CuLaO_2$ must be combined with a couple whose redox potential is close to CB to give rise to a large B-value. S^{2-} and $SO_3{}^{2-}$, differing by their potentials, suitably biased the oxide to form a SCR. Absorption of light by $CuLaO_2$ promotes electrons into CB (−1.99 V) sufficient to reduce H_2O in presence of platinum even in strong alkaline media (E_{red} (H_2O/H_2) = −0.20 V).

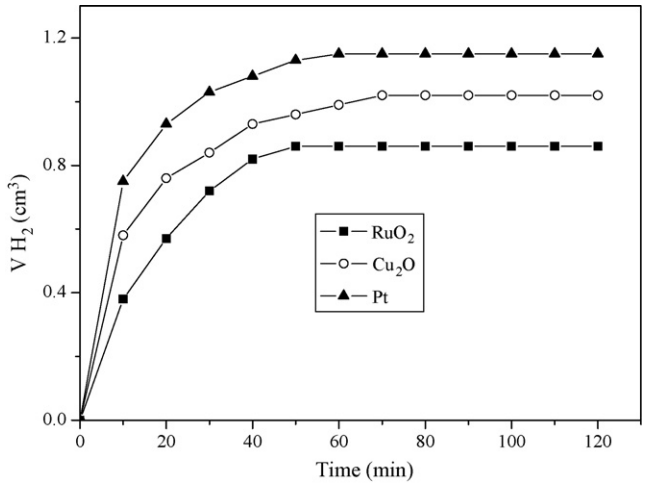

Fig. 7. Volume of evolved H_2 vs. time in S^{2-} 0.5 M/KOH 1 M over the heterosystem $CuLaO_2$/CE.

[2] The equivalent physical quantity of V_{fb} is the electron affinity EA ($=\chi - 0.5E_g$). For $CuLaO_2$, the electronegativity χ is the geometrical mean $(\chi_{Cu}\chi_{La}\chi_O{}^2)^{0.25}$.

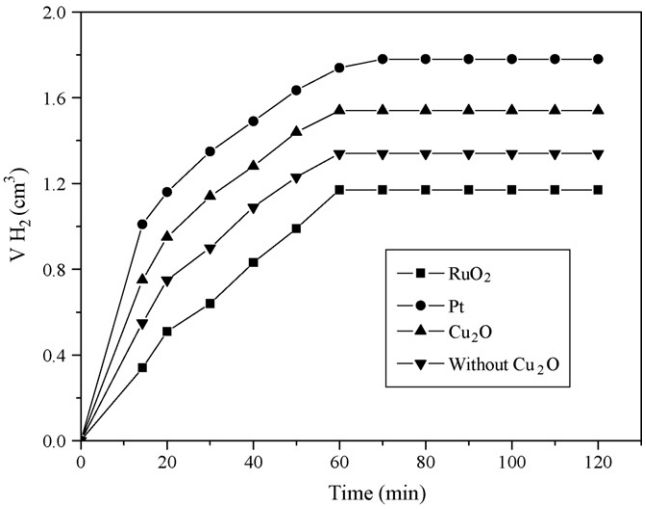

Fig. 8. Volume of evolved H_2 vs. time in SO_3^{2-} 0.5 M/KOH 1 M over the heterosystem $CuLaO_2$/CE.

RuO_2 used as counter electrode showed a negative effect on catalytic activity compared to unloaded oxide probably because of its strong affinity to hydrogen adsorption. To the contrary, the photoactivity was about twice with Pt (Figs. 7 and 8). Indeed Pt has the highest work function (~5.64 eV) [21] and contributes to decrease the barrier potential height of photochemical diode Pt-$CuLaO_2$. Moreover, platinization results in an increase of rate constants of S^{2-} and SO_3^{2-} oxidation (Figs. 7 and 8).

The powder dispersion, technically simple and convenient for practical use, acts as infinity of microphotochemical diodes. The two electrodes are connected to each other in a short circuit configuration; the common potential is close to SO_3^{2-}/Pt system because of its less polarizability. The half electrochemical reactions proceed simultaneously on opposite poles of Pt-$CuLaO_2$ crystallite. Holes have a longer lifetime and high probability of transferring to Pt sites where they oxidize X^{2-} (reactions (3)–(5)) whereas the electrons migrate in opposite direction to the oxide/solution interface to reduce water into gaseous hydrogen reaction (6), the circuit is then closed electrolytically with a negligible resistance. S^{2-} and SO_3^{2-} oxidations, respectively, to S_n^{2-} and $S_2O_6^{2-}$ and in parallel with SO_4^{2-} take place via hole injection in VB located at +0.34 V:

$$nS^{2-} + 2(n-1)h^+ \rightarrow S_n^{2-} (n = 2\text{–}4), \quad E^0 \approx -0.77\,\text{V} \qquad (3)$$

$$2SO_3^{2-} + 2h^+ \rightarrow S_2O_6^{2-}, \quad E^0 \approx -0.22 \qquad (4)$$

$$SO_3^{2-} + 2OH^- + 2h^+ \rightarrow SO_4^{2-} + H_2O, \quad E^0 \approx -1.18 \qquad (5)$$

$$H_2O + 2e^- \rightarrow H_2 + 2OH^-, \quad E^0 \approx -0.20 \qquad (6)$$

As reported earlier [13], the oxidation of SO_3^{2-} into SO_4^{2-} (reaction (5)) consumes OH^- ions and their concentration near the interface is smaller than that of SO_3^{2-}. Consequently the amount of sulfate SO_4^{2-} remains low and the formation of dithionate (reaction (4)) is favored.

The influence of pH is on one hand that of controlling of free species X^{2-}. The pH dependence of H_2-production are shown in Figs. 9 and 10. For S^{2-}, a maximal value was obtained at pH 13.7

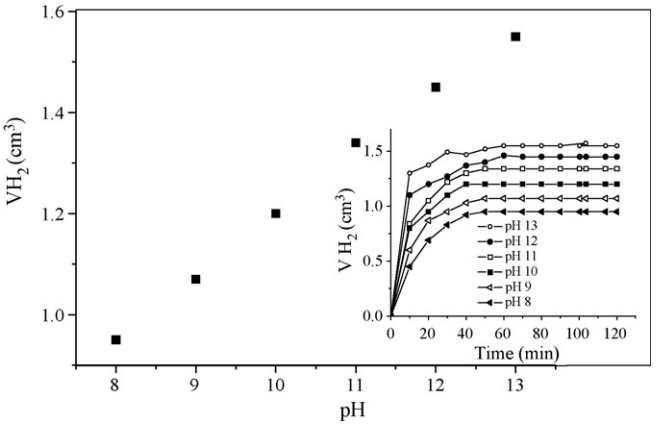

Fig. 9. pH dependence of H_2 over platinized $CuLaO_2$ in S^{2-} 0.5 M/KOH 1 M. Insert the H_2 evolution vs. time at various pH.

where the reduction ability of photoelectrons in CB should permit an efficient carriers transfer and the photoactivity decreases progressively to zero near pH 7. In 1 M KOH, predominantly S^{2-} species were present because of the second acidity constant of H_2S ($pK_{a2} = 11.96$) [21]. The negligible activity at pH < 7 is attributed to the disadvantage energetics for the reduction of H_2O which exhibits a more positive potential; it become far away $CuLaO_2$-CB inhibiting the electron exchange. On the contrary, the conversion rate of SO_3^{2-} peaked at pH 8 and decreases in both directions. Lower pHs favors the competitive reduction (5) as demonstrated early [22]. The reduction of SO_3^{2-} takes place more easily over platinum than H_2O and seems to be the reason of the low photoactivity. The $J(V)$ plots of SO_3^{2-} correlate this feature (Fig. 11), the reduction wave which is proportional to SO_3^{2-} concentration increases with decreasing pH. At high pH, the regression of the photoactivity is attributed to the potential shift of H_2O/H_2 level towards the cathodic direction which decreases the bending B at the interface and increases the recombination process.

An efficient electrochemical system must have a large exchange current density (i_0), a low Tafel slope $\partial \log i/\partial V$ and a small polarization resistance (R_p). Although the potential of

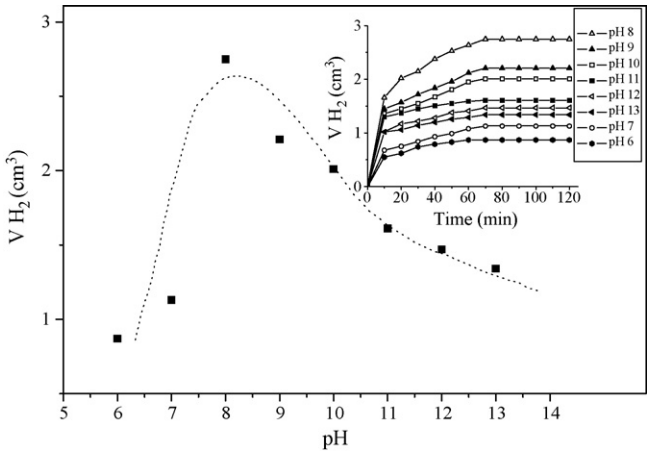

Fig. 10. pH dependence of H_2 over platinized $CuLaO_2$ in SO_3^{2-} 0.5 M/KOH 1 M. Insert the H_2 evolution vs. time at various pH.

Table 3
The kinetic parameters of $CuLaO_2$ with S^{2-} and SO_3^{2-}

X^{2-}	$B = \lvert V_{fb} - E^0_{red} \rvert$ (V_{sce})	i_0 (mA cm^{-2})	$\delta (\log i)/\delta V$	R_p (Ω)
SO_3^{2-}	1.32 (SO_3^{2-}/SO_4^{2-})	0.24×10^{-6}	Anode: 44.7, 4.5133	747
S^{2-}	0.91	10^{-6}	Anode: 43.4, 0.9375, 2.4220	240

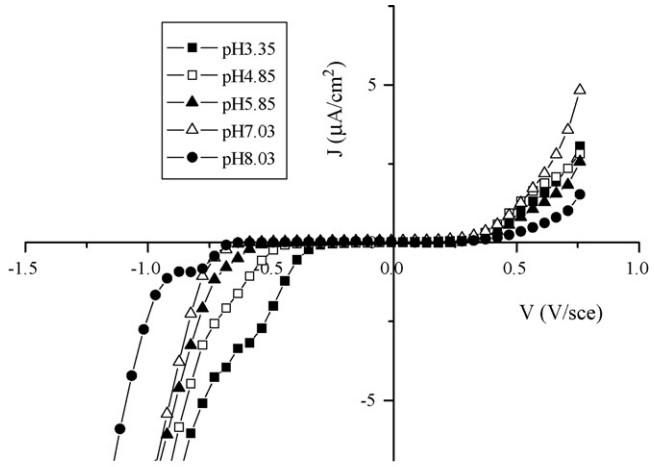

Fig. 11. The $J(V)$ curve over Pt electrode. Electrolyte SO_3^{2-} (0.025 M) with various pH, scan rate 5 mV s^{-1}.

S_n^{2-}/S^{2-} couple is lower than that of $SO_3^{2-}/S_2O_6^{2-}$ and should theoretically give rise to a large B-value, the best photoactivity with the latter couple can be explained from kinetic considerations (Table 3). Light induced SO_3^{2-} conversion involves two mechanisms, it is oxidized simultaneously to $S_2O_6^{2-}$ and SO_4^{2-} since the potential $SO_4^{2-}/S_2O_6^{2-}$ couple (+2.14 V) is far above VB and cannot be involved through VB process in spite of a large O_2-overpotential over $CuMO_2$. This was supported by dual slopes in semi-logarithmic plots (Fig. 12). The results of Table 3 are contrasted to the expected tendency, i.e. the system SO_3^{2-}/Pt exhibits a larger R_p and a lower slope although the photoactivity is greatest with SO_3^{2-}.

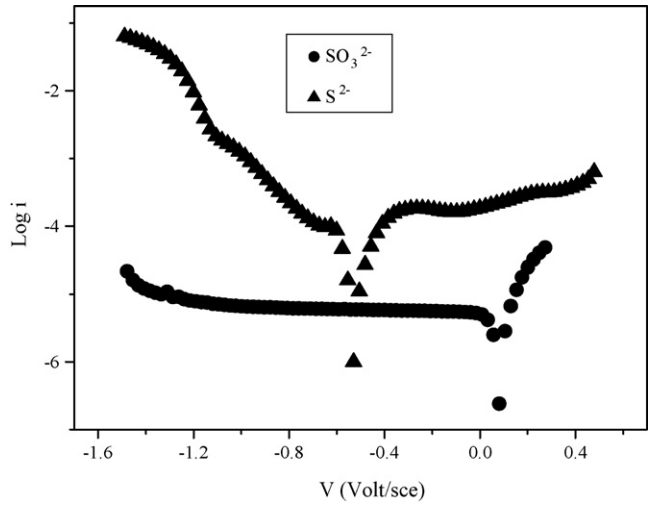

Fig. 12. Semi-logarithmic plots over Pt electrode in S^{2-} and SO_3^{2-} electrolytes at a scan rate of 5 mV/s.

Keeping in mind the low electron mobility in delafossite oxides due to narrow Cu 3d bands and carrier trapping at grain boundaries, the rate of overall PEC process will be that of the slowest step. The transport of species in solution is fast enough to keep the electron concentration near $CuLaO_2$ interface well below a critical value particularly with small polarons SC, a feature corroborated by the constancy of J_{ph} under a vigorous agitation of the solution. In a closed reactor, the accumulated S_n^{2-} and $S_2O_6^{2}$ species are not renewed and leads to a stationary state limiting the amount of evolved H_2. In addition, both species compete with H_2O reduction and shoots up the rate of back reactions (3) and (4). The tendency towards saturation is due partly due to the strong light absorption of yellow S_n^{2-} which increases with the sulfur chain n where the absorption A follows the empirical law $A \sim 0.0648n$ [23]. The transmission of S_n^{2-} solution is low in the visible region of spectrum, only 20% of light is transmitted for 11 mm path at 490 nm and 15% at 520 nm. The net saturation of the H_2-formation can also be ascribed to the shift of the redox potential towards cathodic direction because of the increase of the H_2-partial pressure.

S^{2-} and SO_2 are produced in large quantities as waste products as well as a nucleation agent in atmosphere and their photoconversion over new catalysts to environmentally less harmful forms is of practical significance. $CuLaO_2$ seems worthy to further exploration by increasing its electrical conductivity. It will serve as starting material for a further heat treatment to prepare a new variety of $CuLaO_{2.62}$ (referred to as Φ-phase) with a newly Cu^{2+} coordinated, promising for H_2-photoelectrode. The excess of oxygen can fill the empty sites in the close packed oxygen lattice and contributes to an increase of EA, an approach to enhance the light response into the visible and IR regions and to increase the resistivity, two features generally contradictory in oxides. Experiments are presently under investigation and issues are being considered in ongoing work.

4. Conclusion

Research into developing new photocathode materials has been directed towards delafossite oxides. $CuLaO_2$, synthesized by direct reaction under oxygen-free atmosphere, was characterized structurally and photoelectrochemically. It has proved to be quite attractive with regard to its chemical stability. The VB consists of non-bonding Cu 3d orbital and the corrosion is less pronounced. Synthesis of doped $CuLaO_2$ onto the La-site was unsuccessful even with Ca of similar size. The position of CB was predicted empirically and confirmed experimentally because of the slightly oxygen over-stoichiometry. The electronic bands are not fixed with respect to the solution and the energetic position of CB is favorable to H_2O reduction in basic media under visible light. The photochemical system for H_2-

production based on p-$CuLaO_2$ in contact with aqueous S^{2-} or $SO_3{}^{2-}$ solutions was studied in connection with some physical parameters. Unloaded oxide exhibited poor performance and changing the metal catalyst from free to Pt made an enhancement in the photoactivity by overcoming a potential barrier and increasing the rate constants of S^{2-} and $SO_3{}^{2-}$ over platinum. Both species provide large band bending and the losses of (e^-/h^+) pairs by recombination are neglected. The difference in their behavior was found to be the lack of reversibility of $SO_3{}^{2-}/S_2O_6{}^{2-}$ couple over platinum and the oxidation of $SO_3{}^{2-}$ follows a successive oxidation scheme. Interfacial reactions can be controlled exclusively by the supply of electrons at the interface because of their low mobility. Over time, the photoactivity stabilized and stayed seemingly at zero. The saturation was due to electrochemical back reductions of $S_n{}^{2-}$ and $S_2O_6{}^{2-}$ in competition with H_2O and to the intense color of $S_n{}^{2-}$ which goes parallel to the amount of produced H_2. $SO_3{}^{2-}$ is an important pollutant and its photoconversion over $CuLaO_2$ is potentially of practical interest. Further work on oxidation of $CuLaO_2$ is being carried out and the results will be forthcoming.

Acknowledgments

The authors are indebted to the Faculty of Chemistry (Algiers) for the financial support under the contract no. E 1607/07/06 and would like to thank Mr B. Biri for his technical assistance.

References

[1] A. Kudo, Int. J. Hydrogen Energy 31 (2006) 197–202.
[2] D. Li, J. Zheng, Z. Zou, J. Phys. Chem. Solids 67 (2006) 801–806.
[3] N. Meng, K.H.L. Michael, Y.C.L. Dennis, K. Sumathy, Renew. Sust. Energy Rev. 11 (2007) 401–425.
[4] K. Akihiko, Int. J. Hydrogen Energy 31 (2006) 197–202.
[5] S. Saadi, A. Bouguelia, M. Trari, Sol. Energy 80 (2006) 272–280.
[6] H. Gerischer, Semiconductor Electrochemistry, in: H. Eyring, D. Henderson, W. Jost (Eds.), Topics in Physical Chemistry, vol. 9A, Academic Press, New York, 1970, pp. 463–542.
[7] K.S. Raja, V.K. Mahajan, M. Misra, J. Power Sources 159 (2) (2006) 1258–1265.
[8] E. Mugnier, A. Barnabé, P. Tailhades, Solid State Ionics 177 (2006) 607–612.
[9] M.A. Marquardt, N.A. Ashmore, D.P. Cann, Thin Solid Films 496 (2006) 146–156.
[10] M. Trari, A. Bouguelia, Y. Bessekhouad, Sol. Energy Mater. Sol. Cells 90 (2006) 190–202.
[11] H. Gerisher, Topics in Applied Physics Solar Energy Conversion, Solid State Physics Aspects, Springer–Verlag, Berlin, Heidelberg, New York, 1979, pp. 115–172.
[12] D.E. Aspnes, A. Heller, J. Phys. Chem. 87 (1983) 4949.
[13] J.F. Reber, K. Meier, J. Phys. Chem. 88 (1984) 5903–5913.
[14] M. Elazhari, A. Ammar, M. Alaatmani, M. Trari, J.P. Doumerc, Eur. J. Solid State Inorg. Chem. 34 (1997) 503–509.
[15] N. Koriche, A. Bouguelia, A. Aider, M. Trari, Int. J. Hydrogen Energy 30 (2005) 693–699.
[16] A. Jacob, C. Parent, P. Boutinaud, G. Le Flem, J.P. Doumerc, A. Ammar, M. Elazhari, M. Elaatmani, Solid State Commun. 103 (1997) 529–532.
[17] R.D. Shannon, Acta Crystallogr. A 32 (1976) 751–767.
[18] F.A. Benko, F.P. Koffyberg, Can. J. Phys. 63 (1986) 1306.
[19] F.A. Benko, F.P. Koffyberg, Mater. Res. Bull. 21 (1986) 753–757.
[20] M. Younsi, A. Aider, A. Bouguelia, M. Trari, Sol. Energy 79 (2005) 574–580.
[21] D.R. Lide (Ed.), Electron Work Function of the Elements, Handbook of Chemistry and Physics, 78th ed., Florida, 1997–1998, pp. 12–124.
[22] D.D. Perrin, in: D.R. Lide (Ed.), Ionization Constants of Inorganic Acids and Bases in Aqueous solution, Handbook of Chemistry and Physics, 78th ed., Florida, 1997–1998, pp. 8–43.
[23] S. Saadi, A. Bouguelia, M. Trari, Renew. Energy 31 (2006) 2245–2256.